

MOX-Report No. 46/2025

On the Impact of Light Spectrum on Lettuce Biophysics: A Dynamic Growth Model for Vertical Farming

Mirabella, S.; David, E.; Antona, A.; Stanghellini, C.; Ferro, N.; Matteucci, M.; Heuvelink, E.; Perotto, S.

MOX, Dipartimento di Matematica Politecnico di Milano, Via Bonardi 9 - 20133 Milano (Italy)

mox-dmat@polimi.it

https://mox.polimi.it

On the Impact of Light Spectrum on Lettuce Biophysics: A Dynamic Growth Model for Vertical Farming

Susanna Mirabella¹, Etienne David², Alessandro Antona², Cecilia Stanghellini³, Nicola Ferro⁴, Matteo Matteucci⁵, Ep Heuvelink⁶, Simona Perotto¹

August 10, 2025

¹MOX-Department of Mathematics, Politecnico di Milano
Piazza Leonardo da Vinci 32, I-20133, Milano, Italy
 ²Agricola Moderna, Via Sandro Pertini 26, I-20066, Melzo, Italy
 ³Wageningen University and Research, Greenhouse Horticulture and Flower Bulbs Unit,
Droevendaalsesteeg 1, 6708 PA, Wageningen, the Netherlands
 ⁴Department of Molecular Sciences and Nanosystems, Ca' Foscari University of Venice,
Campus Scientifico, Via Torino 155, Venezia Mestre, I-30172, Italy
 ⁵Department of of Electronics, Information and Bioengineering, Politecnico di Milano
Piazza Leonardo da Vinci 32, I-20133, Milano, Italy
 ⁶Horticulture and Product Physiology, Department of Plant Sciences, Wageningen University,
Droevendaalsesteeg 1 6708 PB Wageningen, the Netherlands

Abstract

Current crop growth models, whether process-based or data-driven, rarely incorporate spectral light composition, limiting their applicability in highly controlled environments such as vertical farming. This work addresses this gap by adjusting a well-established process-based model for lettuce growth with an explicit, data-driven representation of light spectrum effects. Using explainable machine learning techniques, we identify the most relevant spectral features, specifically the Blue:Red and FarRed:Red ratios, and integrate them into a new model parameter, γ , which captures their physiological impact on plant development. The resulting adjusted model (aVH_{opt}) is then validated on an independent literature dataset, showing a substantial reduction in prediction error compared to the reference state-of-the-art model, with a more than 60% decrease in RMSE. The application of the aVH_{opt} model to a commercial dataset confirms its capability to capture key spectral effects, but also reveals its sensitivity to environmental and biological variability not fully accounted for in the current formulation.

1 Introduction

Due to demographic, environmental, and economic factors, traditional farming systems face an urgent need for innovative agricultural practices and technologies in order to improve efficiency, sustainability, and resilience to changing global conditions [1, 2, 3, 4, 5].

Vertical farming, a branch of Controlled Environment Agriculture (CEA), has emerged as an innovative approach to produce fresh vegetables year-round near metropolitan areas. It ensures consistent quality and yield, regardless of weather or climate change, offering a local solution to the food demands of growing urban populations. Vertical farming involves cultivating crops in vertically stacked layers and relies on a range of advanced technologies, including sensors, artificial intelligence, robotics, and automated hydroponic systems [6]. Environmental parameters such as temperature, humidity, CO₂ concentration, and light spectrum composition are precisely controlled using dedicated systems [7, 8].

In particular, despite the technological aspects of vertical farming have advanced, the effectiveness of crop production in such systems largely depends on understanding plant growth in response to controllable environmental variables [9]. To this end, mathematical models offer significant benefits by providing a structured approach to effectively describe and quantify plant-environment interactions, for instance to forecast crop yields, simulate the impact of environmental factors, understand the physiological processes driving plant growth. Among the crop models available in the literature, we distinguish two main categories:

- process-based models. These models use equations to represent crop physiological processes and their interaction with the environment, incorporating principles like photosynthesis, respiration, transpiration, and nutrient uptake. The main strength of this kind of models is high interpretability, making them valuable for hypothesis testing and assessing physiological responses to stressors. However, process-based models demand detailed knowledge of the crop system, often filled in with empirical parameters. As a result, they require calibration and validation, which can be resource-intensive, and may miss unexpected behaviors not explicitly modeled.
- data-driven models. These models use statistical or machine learning methods to predict crop growth from historical data, identifying patterns among factors like light, temperature, humidity, and nutrients without modeling biological mechanisms. The associated strengths lie in flexibility, rapid development once data is available, and the ability to capture complex, non-linear relationships. However, the "black box" nature of data-driven models reduces interpretability, limiting insight into underlying causes. The performance of data-driven models also heavily depends on data quality and may not generalize well to unseen conditions.

Most existing crop growth models are predominantly developed for open-field or green-house cultivation, where environmental variables exhibit limited controllability. This contrasts significantly with modeling approaches in highly controlled environments, such

as vertical farming systems. As an example, in this context, light management critically influences photosynthesis, plant morphology, and biomass accumulation, thereby affecting yield, product quality, and the overall energy efficiency of the agricultural system. With a specific focus on lettuce cultivation, recent research has extensively investigated the effects of various light ratios on plant growth by precisely manipulating individual spectral components. These include blue, green, and far-red light relative to red light, which represents the primary driver of photosynthetic activity [10, 11, 12]. The literature contributions specifically highlight the impact of Blue:Red (B:R), Green:Red (G:R), and FarRed:Red (FR:R) ratios, often distinguishing between:

- B:R effect. Red light is responsible for the highest quantum yield, particularly at low intensities [13], and is known to promote biomass accumulation, plant height, leaf width, and leaf size [14, 15, 16]. In contrast, blue light can inhibit growth, but plays a crucial role in ensuring normal plant morphology, promoting plant compactness [17, 18, 19, 15]. Therefore, the identification of an optimal B:R light ratio is essential to maximize crop performance, balancing rapid leaf expansion, necessary to maximize radiation capture, with prevention of excessive stem elongation [20]. Several studies have addressed the B:R effect, consistently highlighting that a minimum blue light threshold is necessary to support healthy development [21, 18, 19, 22].
- G:R and FR:R effect. Although red and blue light are sufficient for plant production, green and far-red light also play important roles, influencing pigment content, plant morphology, and light capture [11, 23, 24].

 Increasing the G:R ratio supports elongation and photon capture, slightly increasing fresh weight although leading to a minimal impact on dry weight [25]. Its effects are species-dependent, being beneficial for crops like lettuce and microgreens, while less effective (or even detrimental) for others like basil and tomato [25]. Higher FR:R ratio values enhance photosynthetic efficiency by improving the use of shorter wavelengths and triggering shade-avoidance responses. Additionally, FR:R ratio has been shown to increase dry weight independently of the B:R ratio [26], even though the benefits are reduced at high planting densities due to increased competition [27, 28].

Current process-based and data-driven models in the literature related to greenhouse cultivation rarely incorporate spectral variability, thus limiting their applicability in modeling a finely tunable system, such as vertical farming. The aim of this work is thus to introduce an explicit description of the impact of the light spectrum on lettuce growth in a process-based model, supported by and successively improved through a data-driven approach. The proposed enhanced model includes the following steps:

1. identification of the most important light-related features to describe the impact of the light spectrum on the plant growth. This task is carried out by applying explainable machine learning techniques either onto the well-established E.J. Van

Henten dynamic lettuce growth model described in Section 2.1 and onto experimental datasets (Section 2.2);

- 2. proposal of the adjusted model to include the prominent light-related features identified in step 1 (Section 2.3);
- 3. optimization (Section 2.3) of the parameters characterizing the adjusted model through the data in Section 2.2;
- 4. validation (Section 3) of the adjusted model on the dataset in [11];
- 5. analysis of potential limitations of the adjusted model through machine learning algorithms onto more extensive commercial datasets (Section 4).

2 Materials and methods

This section presents the original model proposed in [29] to describe the dry weight growth of a lettuce crop while highlighting the associated limitations when applied to vertical farming systems. Then, we describe the experiments conducted to collect data for adjusting this reference model to account for light spectrum effects. Finally, the adjusted model is proposed and analyzed.

2.1 The original lettuce crop growth model

The Van Henten (VH) model presented in [29] assumes that, at a given time, a one m²-lettuce crop is described by the non-structural, X_{NSDW} [gm⁻²], and the structural, X_{SDW} [gm⁻²], dry weight, so that $X_{DW} = X_{NSDW} + X_{SDW}$ defines the total dry weight.

The dynamic behavior of the two state variables, X_{NSDW} and X_{SDW} , is described by a system of two coupled ordinary differential equations (ODEs), which takes into account the intensity of the incident photosynthetically active radiation U_{PAR} [μ mol m⁻²s⁻¹] (i.e., the photon flux density)¹, the carbon dioxide concentration U_{CO_2} [ppm] and the air temperature U_T [°C]. In particular, the reference VH model reads as

$$\begin{cases} \dot{X}_{NSDW} = c_{\alpha} f_{phot} - r_{gr} X_{SDW} - f_{resp} - \frac{1 - c_{\beta}}{c_{\beta}} r_{gr} X_{SDW} \\ \dot{X}_{SDW} = r_{gr} X_{SDW}, \end{cases}$$
(1)

where: $c_{\alpha}f_{phot}$ models the rate of conversion of assimilated CO₂ into sugar CH₂O by means of light energy (i.e., the photosynthesis process), with c_{α} the ratio (equal to 30/44 = 0.68) of the molecular weights of CH₂O and CO₂, and f_{phot} the gross canopy photosynthesis; $r_{gr}X_{SDW}$ is related to the conversion rate from non-structural to structural dry weight (i.e., the SDW growth process), with r_{gr} the specific growth rate coefficient; f_{resp} coincides with the maintenance respiration rate, which provides energy

¹To be consistent with the data involved in the experiments, we replace the standard unit measure $[Wm^{-2}]$ with $[\mu mol m^{-2}s^{-1}]$ following [30].

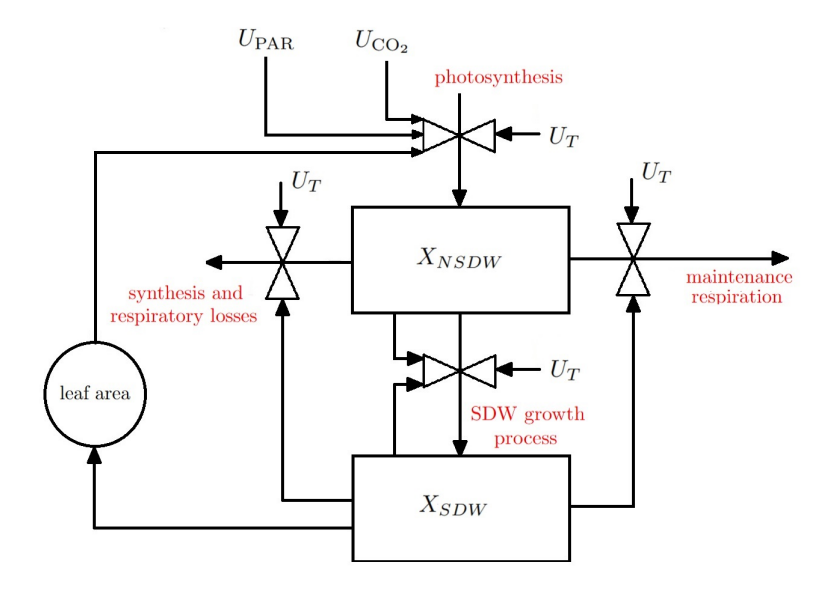


Figure 1: Relational diagram for the lettuce crop growth model (1).

to preserve cells in terms of biostructure and ionic gradients; $(1-c_{\beta})r_{gr}X_{SDW}/c_{\beta}$ refers to the synthesis and respiratory losses due to growth, with c_{β} the associated coefficient. Finally, system (1) is closed with appropriate initial conditions.

The relational diagram in Figure 1 provides a compact representation of system (1). In more detail, the state variables X_{NSDW} and X_{SDW} are highlighted in the boxes; the model inputs are U_T , U_{CO_2} , U_{PAR} ; the main four growth rates involved in (1) are represented as valves, while the arrow direction depends on the income/outcome nature of the contribution (i.e., on the corresponding sign in (1)); the leaf area represents an auxiliary variable and is depicted in the circle.

The validation of equations (1) carried out in [29] corroborates the reliability of the reference model in a greenhouse environment. Vice versa, the application of the VH model in a vertical farming context immediately highlights two main issues, i.e., crops are grown under a single light quality (solar radiation) and geometric properties of the canopy with respect to incident radiation are considered static. Indeed, in vertical farming, seeding density can be considerably high and the intensity of each light band can be modulated depending on the specific growth needs. In the following, we focus on the latter issue with the aim to adapt the original model to vertical farming cultivation systems.

2.2 Experiment description

This section details the experiment setting at the basis of the proposed adjusted Van Henten (aVH) model.

The experiments were conducted at Agricola Moderna, a vertical farming company based in Melzo (Milan), Italy. The company production facility consists of two 8-layer climate



Figure 2: Lettuce plants (variety 62) under a red-blue spectrum at 180 $[\mu \text{mol m}^{-2}\text{s}^{-1}]$ with B:R= 0.5: lettuce growth at 6 (left), 15 (center), 27 (right) days after the germination, at a low (top) and high (bottom) planting density.

cells, characterized by different average temperature conditions. We study two planting densities, low (one plant per pot) and high (two plants per pot)², across three different varieties of *Lactuca sativa L.*, namely crispy, blond and green incised crispy below labeled as 62, 259, and 453, respectively.

All cultivation cycles are conducted in the same layer of the same cell to minimize the effect of temperature variations across different areas, possibly resulting from proximity to exit doors or to the ventilation system.

Day/night temperature is set to 26/22 [°C], with a CO₂ concentration maintained at 750 [ppm]. The photoperiod is selected in order to provide a 20-hour light cycle with a total light intensity equal to 180 [μ mol m⁻²s⁻¹], followed by a 4-hour dark cycle.

Each growing cycle starts with a three-day germination period in a dark chamber, followed by a growth phase into an ebb and flow system lasting 27 days.

We refer to Figure 2 for some pictures detailing the experiments.

2.2.1 Experimental design and light treatments

We investigate 8 different light treatments characterized by the same total light intensity, comprising different proportions of Blue (400–500 [nm]), Green (500–600 [nm]), Red (620–680 [nm]), FarRed (700–750 [nm]) light bands, as detailed in Table 1.

2.2.2 Data collection

For each light treatment, we randomly pick 12 plants retrieved from one tray per variety containing either 24 (low density) or 48 (high density) individuals (see Figure 2). The collected data do coincide with the values of average fresh and dry mass measured at

 $^{^2}$ The specific plant density [plants m $^{-2}$] is not disclosed for confidentiality reasons.

Table 1: Different light treatments involved in the data collection phase at Agricola Moderna.

Treatment	В	\mathbf{G}	\mathbf{R}	\mathbf{FR}	$\mathbf{B}\%$	$\mathbf{G}\%$	$\mathbf{R}\%$	$\mathbf{FR}\%$	B:R	G:R	FR:R
1	90	0	90	0	50	0	50	0	1.00	0.00	0.00
2	0	0	180	0	0	0	100	0	0.00	0.00	0.00
3	15	0	165	0	8	0	92	0	0.09	0.00	0.00
4	30	0	150	0	17	0	83	0	0.20	0.00	0.00
5	60	0	120	0	33	0	67	0	0.50	0.00	0.00
6	22	34	110	14	12	19	61	8	0.20	0.31	0.14
7	22	34	122	2	12	19	68	1	0.18	0.28	0.02
8	22	0	144	14	12	0	80	8	0.15	0.00	0.10

day 7, 15, 21, and 27 (harvest time), where the dry mass is obtained by drying the leaves in a ventilated oven at 130 [°C] for 7 hours.

2.2.3 Additional dataset

The data collected during the collaboration with Agricola Moderna include a wide variety of treatments in terms of B:R ratio, while providing insufficient insight about the effect of FR:R ratio. To address this limitation, an additional dataset is used with a view to a reliable model calibration. We exploit the data associated with a set of experiments carried out at the University of Bologna [12], under conditions similar to those at Agricola Moderna.

All growth cycles are conducted for Lactuca sativa L., in particular the Canasta variety, at a planting density of 153 [plants m⁻²]. The light intensity is kept fixed at 200 [μ mol m⁻²s⁻¹] across five distinct treatments, by maintaining a constant B:R ratio while varying the proportion of FR light in the spectrum. A summary of the light treatments is provided in Table 2.

The photoperiod is set to a 16-hour light/8-hour dark cycle, with temperatures maintained between 21 [°C] and 24 [°C], and with a CO₂ concentration equal to 850 [ppm]. The crops are sampled after 8, 15, 22, and 29 (harvest time) days, when the associated fresh and dry weights are measured, along with additional quantities of interest.

2.3 The adjusted model

The adjustment of the original VH model moves from an analysis of the available literature. The impact of the light spectrum on plant growth and development has been widely studied in plant physiology, resulting in numerous comparative experiments and statistical analyses [18, 31, 32, 33]. These studies highlight how light quality impacts the processes explicitly modeled in (1) (e.g., photosynthesis and respiration) and related physiological responses (e.g., stomatal development, leaf expansion, plant morphology).

Table 2: Different light treatments involved in the data collection phase at University of Bologna [12].

Treatment	В	\mathbf{G}	R	\mathbf{FR}	$\mathbf{B}\%$	$\mathbf{G}\%$	$\mathbf{R}\%$	$\mathbf{FR}\%$	B:R	G:R	FR:R
1	50	0	150	0	0.25	0.00	0.75	0.00	0.33	0.00	0.00
2	47.5	0	142.5	10	0.23	0.00	0.71	0.05	0.33	0.00	0.07
3	42.5	0	127.5	30	0.21	0.00	0.63	0.15	0.33	0.00	0.23
4	37.5	0	112.5	50	0.18	0.00	0.56	0.25	0.33	0.00	0.44
5	32.5	0	97.5	70	0.16	0.00	0.48	0.35	0.33	0.00	0.72

We propose to introduce a parameter, γ , to quantify how different light band combinations influence non-structural dry weight production, so that we modify (1) into

$$\begin{cases} \dot{X}_{NSDW} = \gamma \left(c_{\alpha} f_{phot} - r_{gr} X_{SDW} - f_{resp} - \frac{1 - c_{\beta}}{c_{\beta}} r_{gr} X_{SDW} \right) \\ \dot{X}_{SDW} = r_{gr} X_{SDW}. \end{cases}$$
(2)

In the following, we define γ as a function of appropriately selected spectrum-dependent features. To assess the impact of γ on crop growth prediction, we first analyze the limitations of the calibrated version of the VH model (cVH) on the datasets presented in Section 2.2, which markedly differ from the low-planting-density greenhouse conditions for which the model was originally designed. The cVH model will be also instrumental to carry out a reliable comparison with the aVH model. Notice that cVH and aVH models do coincide for $\gamma = 1$, whereas $\gamma > 1$ ($\gamma < 1$) corresponds to an underestimation (overestimation) of the cVH model with respect to the adjusted one.

The complete workflow for the adjustment of model (1) is detailed in the following sections.

2.3.1 Step 1: selection of light-dependent parameters for the VH model

This phase starts from the definition of the cVH model performed for each lettuce variety separately, by using the data collected at Agricola Moderna and at University of Bologna. The calibration underlying cVH focuses on the parameters related to light usage, for which the original model exhibits a sensitivity greater than 35%. Here, the sensitivity of the model output to a perturbation in parameter p_i is defined as:

$$S_i = \frac{\delta X_{DW}(T_H)}{\delta p_i} \cdot \frac{p_i}{X_{DW}(T_H)},\tag{3}$$

where $X_{DW}(T_H)$ is the simulated total dry weight at harvest time T_H , δp_i denotes a small variation in parameter p_i , and $\delta X_{DW}(T_H)$ is the associated change in dry weight. With reference to the values in Table 3, the criterion adopted for selecting the parameters to be calibrated leads to choose c_{ϵ} (i.e., the light use efficiency at very high CO₂ concentration, originally set to $3.8 \cdot 10^{-5}$ [g μ mol⁻¹]) and c_k (i.e., the light extinction

Table 3: Sensitivity of the VH model with respect to parameters used in [29], setting δp_i to 0.05 in (3). The highlighted parameters are selected for calibration.

p_i	S_i
c_{β}	0.95
c_{ϵ}	0.83
$c_{car,2}$	0.46
c_{lar}	0.38
c_k	0.38
$c_{car,1}$	0.20

p_i	S_i
c_{Γ}	0.19
g_{bnd}	0.16
$c_{Q_{10}resp}$	0.15
$c_{car,3}$	0.14
$c_{gr,max}$	0.14
$c_{resp,sht}$	0.13

p_i	S_i
$c_{Q_{10}rgr}$	0.11
gstm	0.08
c_{τ}	0.06
$c_{Q_{10}\Gamma}$	0.06
$c_{resp,rt}$	0.00

coefficient, originally set to 0.9). On the contrary, we neglect three quantities not related to light usage, namely c_{β} since representing the respiratory and synthesis losses of non-structural material due to growth, $c_{car,2}$ modeling the carboxylation conductance and c_{lar} denoting the structural leaf area ratio.

We observe that parameters c_{ϵ} and c_k are involved in the definition of the photosynthetic rate,

$$f_{phot} = f_{phot}(c_k, c_{\epsilon}; \mathbf{p}) = (1 - e^{-c_k \text{LAI}(\mathbf{p})}) f_{phot, max}(c_{\epsilon}; \mathbf{p}), \tag{4}$$

in system (1), where vector **p** gathers the parameters in Table 3 except for c_{ϵ} and c_k ;

$$LAI = LAI(\mathbf{p}) = c_{lar}(1 - c_{\tau})X_{SDW}$$
 (5)

denotes the leaf area index, with c_{τ} the cultivation-dependent ratio of root to total plant dry mass;

$$f_{phot,max} = f_{phot,max}(c_{\epsilon}; \mathbf{p}) = \frac{\epsilon(c_{\epsilon}) U_{\text{PAR}} g_{\text{CO}_2} c_w (U_{\text{CO}_2} - \Gamma)}{\epsilon(c_{\epsilon}) U_{\text{PAR}} + g_{\text{CO}_2} c_w (U_{\text{CO}_2} - \Gamma)}$$
(6)

the canopy gross CO_2 assimilation rate, assuming full soil coverage and an effective leaf area of 1 m² per m² soil, with

$$\epsilon = \epsilon(c_{\epsilon}) = c_{\epsilon} \frac{U_{\text{CO}_2} - \Gamma}{U_{\text{CO}_2} + 2\Gamma} \text{ [g } \mu \text{mol}^{-1}\text{]}$$
 (7)

the light-use efficiency, computed considering light level impact on CO_2 compensation point and photorespiration, Γ [ppm] being CO_2 compensation point, with g_{CO_2} [m s⁻¹] the conductance to CO_2 diffusion, and c_w [g m⁻³] the density of CO_2 .

For each lettuce variety in the Agricola Moderna and University of Bologna datasets, the parameter calibration is performed using a grid search method to evaluate different combinations of c_{ϵ} , c_k . The goal is to minimize the root mean squared error,

RMSE =
$$\sqrt{\frac{1}{N} \sum_{i=1}^{N} (X_{DW, \text{pred}} - X_{DW, \text{obs}})^2}$$
, (8)

between the N predicted $(X_{DW, pred})$ and observed $(X_{DW, obs})$ dry weights. In particular, to compute $X_{DW, pred}$, we endow problem (1) with initial values for the two state variables

based on the total crop dry weight measured at planting. Following [29], we assume that 75% of the total dry weight is structural. To estimate the dry weight of a single shoot, a sample of shoots from different varieties is measured just after germination, before being transplanted. Thus, it turns out that the average shoot dry weight is about 0.0002 [g]. Multiplying this value by the planting density of each growth cycle gives us the initial total dry weight.

To ensure comparability between the calibration carried out on the University of Bologna and Agricola Moderna datasets, we select a common light treatment as baseline. In particular, the data collected at Bologna University are calibrated using Treatment 1 in Table 2, corresponding to an optimized blue and red spectrum (i.e., B:R = 0.33) according to [12]. Concerning the data collected at Agricola Moderna, we opt for a calibration based on Treatments 4 and 5 in Table 1, which feature a B:R ratio equal to 0.2 and 0.5, respectively. This step provides a calibrated version cVH of the original VH model for each analyzed variety, the associated optimal parameters being collected in Table 4. It can be checked that, on average, RMSE is reduced from 34.6 to 18.5 across all the available growth cycle data. Finally, the left panel in Figure 3 shows the time evolution of X_{DW} for the VH (dashed line) and cVH (solid line) models together with the available experimental data for lettuce variety 62, low planting density, and the two light treatments B:R= 0.2 and B:R= 0.5. The enhancement resulting from the calibration phase becomes particularly evident during the later stages of crop growth. It is worth noting that the stepwise behavior of the X_{DW} curves results from the light being turned off during the night phase, modeled by assigning a piecewise constant profile to U_{PAR} .

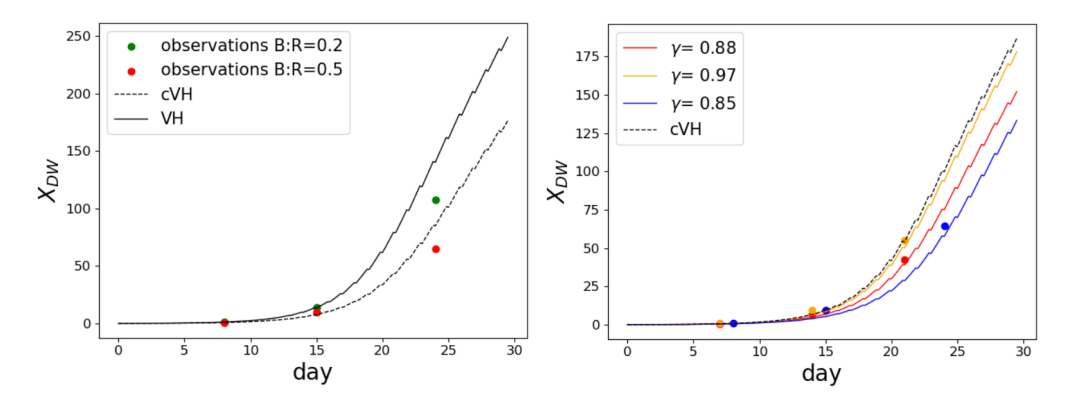


Figure 3: The aVH model: the light spectrum-dependent feature selection step (left); the optimization of parameter γ step (right).

2.3.2 Step 2: optimization of parameter γ for the aVH model

We determine the optimal parameter γ characterizing the adjusted model for each combination of lettuce variety, planting density and light treatment in the two considered datasets. This amounts to consider a total of 53 growth scenarios, namely 3 varieties,

Table 4: Parameter calibration for the cVH model.

Variety	c_k	c_{ϵ}	Dataset
Canasta	0.90	$5.2 \cdot 10^{-5}$	University of Bologna
62	0.78	$3.6 \cdot 10^{-5}$	Agricola Moderna
259	0.69	$4.8 \cdot 10^{-5}$	Agricola Moderna
453	0.87	$3.9 \cdot 10^{-5}$	Agricola Moderna

2 planting densities, 8 light treatments for the experiments at Agricola Moderna and 1 variety, 1 planting density, 5 light treatments for the experiments at University of Bologna. The optimal value of γ is obtained by minimizing the value of the RMSE in (8) with respect to the observed data for each growth setting.

The right panel of Figure 3 shows how X_{DW} evolves over time according to the aVH model for lettuce variety 62 at low planting density. The predictions use the optimal γ values for Treatments 1, 2, and 5, and are compared with the corresponding experimental data. The three model predictions are also compared with the cVH model (dashed line), where no treatment-specific adjustment is applied (i.e., when γ is set to 1). The results show that, unlike the cVH model, the aVH variant more accurately captures the experimental trends across all light treatments. In particular, the three values of γ strictly less than one effectively correct the overestimation observed in the cVH model.

2.3.3 Step 3: identification of high-impact light spectrum components for γ

To better understand the relationship between the light spectrum and the parameter γ in (2), we train a predictive model using a XGBoost regressor [34] and resort to SHAP (SHapley Additive exPlanations) method [35] to quantify the contribution of each spectral feature to the model output γ . To train XGBoost, we relate each of the 53 light spectrum compositions in Section 2.3.2 (i.e., the B:R, G:R, FR:R ratios and the B, G, R, FR percentage with respect to the total light intensity) with the optimal value for coefficient γ , thus taken as target variable.

Figure 4 shows the SHAP values computed for the trained model, thus identifying the light spectrum features that most strongly influence the predicted crop growth response. The x-axis represents the SHAP value associated with each feature of the light spectrum composition. Positive (negative) values indicate how much the feature increases (decreases) the predicted value of γ , quantifying the associated impact on the model output for each of the 53 samples. Each dot highlights a single observation (i.e., one specific combination of lighting condition, density and variety) where the associated color encodes the SHAP value (i.e., from low (blue) to high (red)) of the corresponding feature. We notice that these feature importance analysis results are coherent with current literature [36, 11], demonstrating the relevance of the B:R and FR:R ratios over the other considered light features in explaining lettuce growth dynamics.

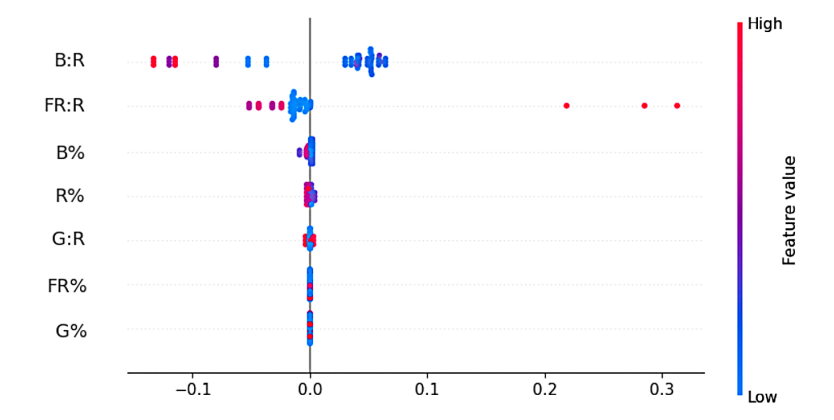


Figure 4: The aVH model: SHAP values associated with the considered features of the light-spectrum composition.

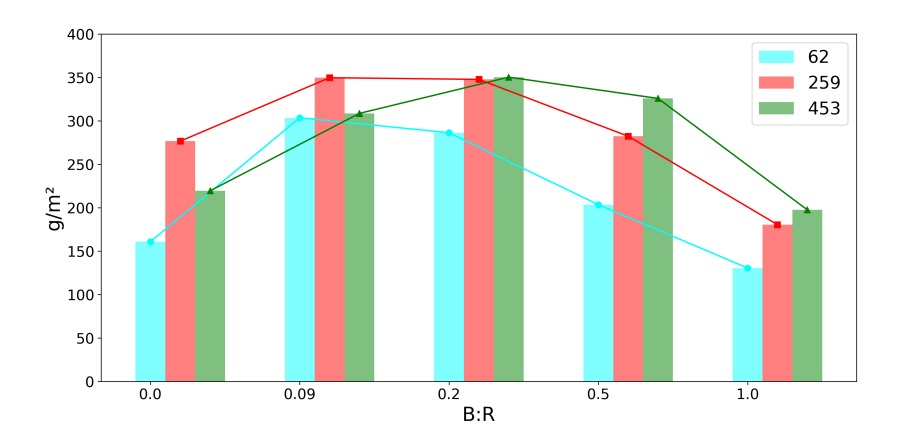


Figure 5: Experimental histograms and corresponding trend of the crop dry weight measured at week 4 as a function of the B:R ratio for lettuce varieties 62, 256 and 453.

2.3.4 Step 4: modeling of the parameter γ

Following the identification of the B:R and FR:R ratios as the most influential components of the light spectrum for determining γ , we model γ as a function of these two ratios, namely

$$\gamma = a_{\text{B:R}} \cdot a_{\text{FR:R}},\tag{9}$$

where $a_{B:R} = a_{B:R}(B:R)$ and $a_{FR:R} = a_{FR:R}(FR:R)$ are functions to be appropriately defined. To this aim, we rely on both the experimental data at our disposal and on state-of-the-art literature concerning the effects of light spectrum on crop growth. In particular, we select studies that align with our reference crop growth conditions, where total photon flux density, photoperiod, CO_2 concentration, and humidity are kept constant while varying the contributions of the light spectrum bands [37, 11, 36, 38, 18, 26, 19, 22, 39].

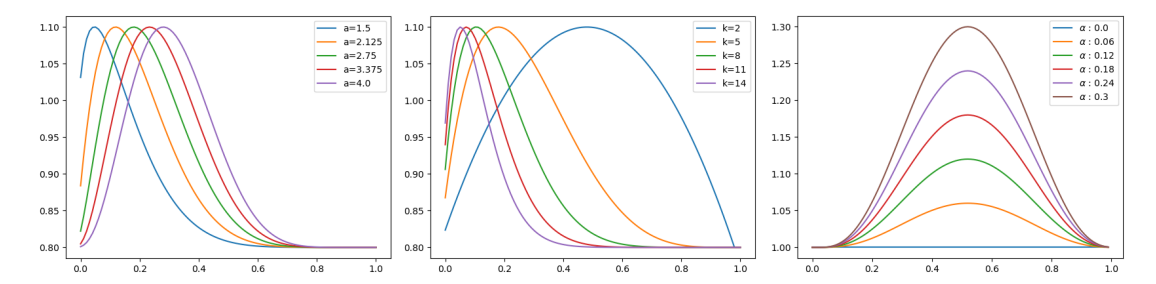


Figure 6: The aVH model: trend of $a_{B:R}$ as a function of the B:R ratio when varying a for k = 8 (left) and when varying k for a = 2 (center); trend of $a_{FR:R}$ as a function of the B:R ratio when varying α for b = h = 4 (right).

Inspired by the trend of dry weight as a function of the B:R ratio shown in Figure 5, we choose a Beta probability distribution as a possible profile for $a_{B:R}$, being

$$\beta(x; a, k) = \frac{\Gamma(a+k)x^{a-1}(1-x)^{k-1}}{\Gamma(a)\Gamma(k)} \quad \text{with} \quad \Gamma(z) = \int_0^\infty t^{z-1}e^{-t} \, \mathrm{d}t, \tag{10}$$

and a and k the distribution shape parameters. In particular, we rescale the Beta distribution to model a sharp decline in biomass accumulation as the B:R ratio increases, with a peak at an intermediate value. We set

$$a_{\text{B:R}} = \tilde{\beta}(\text{B:R}; a, k; m, M), \tag{11}$$

where m and M define the rescaling range, representing the minimum and maximum impact of the B:R ratio on biomass production.

The first two plots in Figure 6 show the behavior of $a_{B:R}$ as a function of B:R. Specifically, the first panel illustrates the effect of varying a (with k = 8 fixed), while the second panel shows the effect of varying k (with a = 2 fixed), when using m = 0.8 and M = 1.1. It is evident that the main effect of parameter a is to shift the peak of the curve along the x-axis, while parameter k primarily controls the width of the peak.

Let us consider now the definition of function $a_{FR:R}$ in (9). Consistently with the bell-shaped trend of the data collected in [12], where the impact of FR:R ratio on lettuce growth is tested while keeping the total light intensity and the B:R ratio constant, we model the FR:R effect by resorting again to the rescaled Beta distribution $\tilde{\beta}$, so that

$$a_{\text{FR:R}} = 1 + \tilde{\beta}(\text{FR:R}; b, h; 0, \alpha), \tag{12}$$

where b, h and 0, α retain the same meaning as a, k and m, M in (11), respectively (we refer to the third panel in Figure 6 for a sensitivity of the $a_{FR:R}$ trend with respect to α). Definition (12) requires that $a_{FR:R}$ takes values greater than or equal to 1, in line with observations from the analyzed growth cycles, where increasing the FR:R ratio had either a positive or negligible effect on plant development³.

³It is important to highlight that the definition of $a_{FR:R}$ is applicable only under low planting densities or during early growth stages (i.e., before week 4). This limitation stems from the lack of reliable data in the literature concerning the impact of FR light at high planting densities and in later phases of growth.

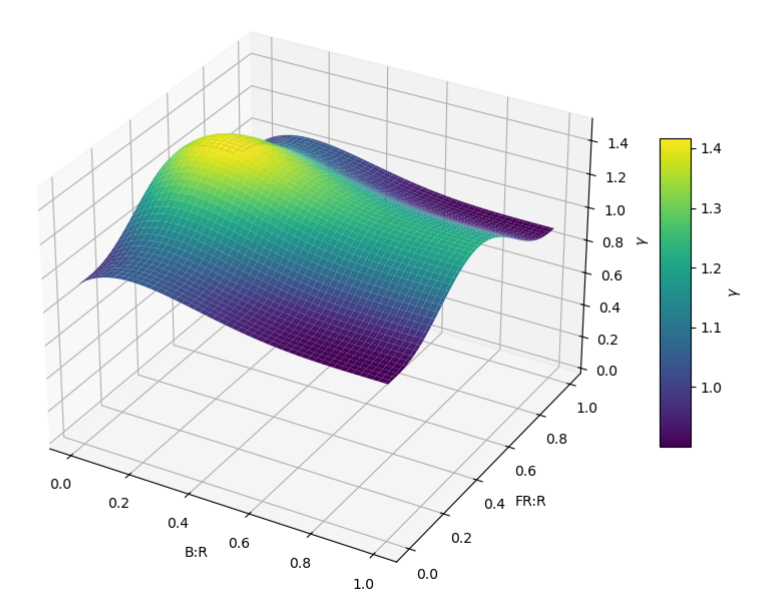


Figure 7: The aVH model: trend of parameter γ in (9) as a function of B:R and FR:R ratios.

The joint effect played by the B:R and FR:R ratios onto the definition of parameter γ according to (9), (11) and (12) is represented by the plot in Figure 7, after setting the aVH model parameters as $a=1.9,\ k=4.6,\ m=0.9,\ M=1.05,\ b=4,\ h=4,\ \alpha=0.35.$ The three-dimensional surface shows a distinct peak at low B:R ratios (around 0.2) and intermediate FR:R ratios (approximately 0.5), suggesting that this spectral combination maximizes the lettuce biomass growth rate. In contrast, both very high and very low values of either ratio lead to a decrease in γ , indicating a reduced effectiveness of the light spectrum in promoting growth, as predicted by the model.

2.3.5 Step 5: definition of the aVH_{opt} model

This phase is performed by using the dry weight measurements during the first three weeks and for all the analyzed varieties, density conditions and light treatment, with the goal of determining the optimal values for the parameters a, k, m, M, b, h, α in (11) and (12). This optimization is carried out in two separate stages:

1. determination of parameters b, h, and α : the computation of these parameters is based exclusively on the experiments conducted at the University of

Bologna, which specifically examine how varying the FR:R ratio affects the growth of Canasta lettuce, while keeping the B:R ratio constant [12]. The optimization of parameters b, h, and α is carried out after fixing c_{ϵ} and c_k in (4) to the corresponding values in Table 4, and by setting $a_{\text{B:R}} = 1$ in (11), since this quantity depends on parameters that will be found in the subsequent stage. Under these assumptions, the optimal values of parameters b, h, and α are computed by minimizing the RMSE in (8) across the observed data for each light treatment in Table 2, covering a total of 5 growth cycles.

2. **determination of parameters** a, k, m, **and** M: the computation of these parameters is undertaken on the dataset collected at Agricola Moderna, since including sufficient variability for the B:R ratio. The optimization of a, k, m, and M assumes for parameters b, h, and α the values yielded by the previous stage, and aims at minimizing the RMSE in (8) across the observed data for all lettuce varieties, density conditions, and light treatments in Table 1, for a total of 48 growth cycles.

The optimal values obtained from these two stages are

$$a = 1.9, k = 4.6, m = 0.9, M = 1.05, b = 4, h = 4, \alpha = 0.35$$
 (13)

(these values are the same as those used in Figure 7). In the following, we refer to the optimized aVH model as the aVH $_{\rm opt}$ model.

3 Results and discussion

This section focuses on the aVH_{opt} model in order to measure the improvement over the cVH model and to test how accurately it reproduces lettuce dry weight dynamics under varying light conditions, based on a new dataset.

Figure 8 shows the RMSE values defined for the four lettuce varieties described in Section 2.2, considering both low and high planting densities for varieties 62, 259 and 453, across all light treatments listed in Tables 1 and 2. The colorbars highlight that the aVH $_{\rm opt}$ model achieves an average RMSE reduction of 31% compared to the cVH model. This confirms that light spectrum composition plays a significant role in crop growth prediction, and that aVH $_{\rm opt}$ effectively accounts for this influence. It is also noteworthy that planting density affects RMSE values, sometimes significantly. In particular, the cVH model tends to perform worse when moving from low to high planting density. In contrast, the aVH $_{\rm opt}$ model shows no clear trend in response to this change. Overall, incorporating sensitivity to plant competition can be beneficial for enhancing predictive capability of the selected crop growth model.

We now evaluate the performance of the aVH_{opt} model on a different dataset, which, however, corresponds to experimental conditions comparable to those described in Section 2.2. Specifically, we use the data from [11], where the authors report crop growth measurements for *Lactuca sativa L.*, cultivars Rex and Rouxai, grown at a planting

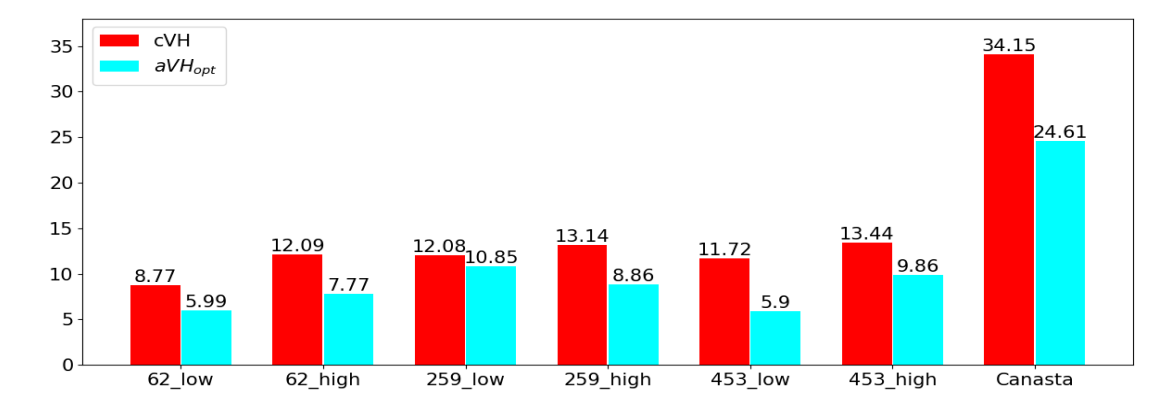


Figure 8: Comparison between the cVH and the aVH_{opt} model in terms of RMSE for different lettuce varieties and planting densities (labeled as variety_density).

density of 200 [plants m⁻²], under a fixed light intensity of 180 [μ mol m⁻²s⁻¹], with a 20-hour light/4-hour dark photoperiod. Temperature is maintained at approximately 20 [°C], with a CO₂ concentration of 450 [ppm].

In the experiments described in [11], lettuce plants are initially grown under warm-white LED light at 180 [μ mol m⁻²s⁻¹] for 9 to 11 days before being transferred to hydroponic systems with various lighting treatments. This preliminary phase helps prevent the negative effects of immediate exposure to pure red light after germination, such as excessive stem elongation and weakened structure (the first three bins in Figure 6 show this problematic trend for the dataset in Section 2.2, consistently with the findings in [40]). Since the optimal values in (13) involve plants grown under pure red light from day one, without a warm-white light phase, the full-red treatments from [11] are not directly comparable and are therefore excluded from the validation process (see Table 5 for details on the specific light treatments considered).

For this dataset, in Table 6, we compare the dry weight predictions obtained from the cVH model (recalibrated on the new data) and from the aVH $_{\rm opt}$ model with the experimental measurements at harvest time, evaluating the RMSE as a function of both the B:R and FR:R ratios. The values in the table highlight that, despite calibration, the cVH model remains unresponsive to changes in light spectrum composition in contrast to the aVH $_{\rm opt}$ model. Across all lighting treatments, aVH $_{\rm opt}$ consistently delivers more accurate predictions of dry weight, reducing the average RMSE from 44.53 to 16.63. Finally, it is worth noting that the B:R and FR:R ratios used in Treatment 3 fall within the region where the surface in Figure 7 reaches its peak. This is reflected in the highest observed dry weight value, which is accurately captured by the aVH $_{\rm opt}$ model. The associated RMSE is significantly lower than that of the cVH model, confirming the improved predictive performance.

Table 5: Different light treatments involved in the data in [11].

Treatment	В	\mathbf{G}	R	\mathbf{FR}	В%	G %	$\mathbf{R}\%$	FR%	B:R	G:R	FR:R
1	20	40	120	0	11	22	67	0	0.17	0.33	0.00
2	20	20	120	20	11	11	67	11	0.17	0.17	0.17
3	20	0	120	40	11	0	67	22	0.17	0.00	0.33
4	40	20	120	0	22	11	67	0	0.33	0.17	0.00
5	40	0	120	20	22	0	67	11	0.33	0.000	0.167
6	60	0	120	0	33	0	67	0	0.50	0.00	0.00

Table 6: Comparison between the cVH and the aVH $_{opt}$ model in terms of dry weight and RMSE for the light treatments in Table 5.

Treatment	B:R	FR:R	$X_{DW, \mathrm{obs}}$	$X_{DW,cVH}$	$X_{DW, aVH_{opt}}$	$RMSE_{cVH}$	$RMSE_{aVH_{opt}}$
1	0.17	0.00	269.6	213.6	253.9	56.0	15.7
2	0.17	0.17	283.4	213.6	247.9	69.8	35.5
3	0.17	0.33	287.6	213.6	312.6	74.0	25.0
4	0.33	0.00	237.4	213.6	227.6	23.8	9.8
5	0.33	0.17	246.4	213.6	241.3	32.8	5.1
6	0.50	0.00	202.8	213.6	211.5	10.8	8.7

4 Application to a commercial dataset: insights and challenges

In this section, we evaluate the performance of the ${\rm aVH_{opt}}$ model on a dataset that differs substantially in characteristics from the one used previously, namely we focus on a commercial dataset. In general, there is a clear distinction between research and commercial data. While the former offer detailed trait measurements under controlled or even extreme conditions, they are limited in scale due to the cost and destructiveness of sampling. In contrast, commercial datasets cover many more growth cycles and reflect real production environments, but include fewer measurements per cycle and often rely on indirect, non-destructive methods, which may introduce additional uncertainty.

For this analysis, we rely on an extensive commercial dataset provided by Agricola Moderna, which documents multiple growth cycles of a specific lettuce variety cultivated under a range of environmental conditions. These include some of the scenarios used to optimize the aVH model, as well as additional growth conditions not previously considered. The dataset contains detailed records for 424 growth cycles of variety 62, all conducted at high planting density. Each cycle was carried out under the same photoperiod (20-hour light/4-hour dark) and identical light conditions, with a total intensity of 225 [μ mol m⁻²s⁻¹] and spectral composition of 12% Blue, 19% Green, 61% Red, and 8% FarRed. The CO₂ concentration was kept constant at 750 [ppm] throughout the facility.

For each cycle, the dataset includes the following measurements: dry weight at harvest, growth cycle duration, time series of temperature and relative humidity (sampled every 30 minutes), available substrate per plant, and the crop's location within the vertical farming cell (i.e., layer and table position). This makes the dataset a valuable source of real-world production data, capturing both biological performance and environmental context. It is important to note, however, that the dataset exhibits a degree of spatial heterogeneity. Due to the fixed position of ventilation systems and air inlets, variations in temperature, humidity, and airflow can occur depending on the crop's position within the growing chamber.

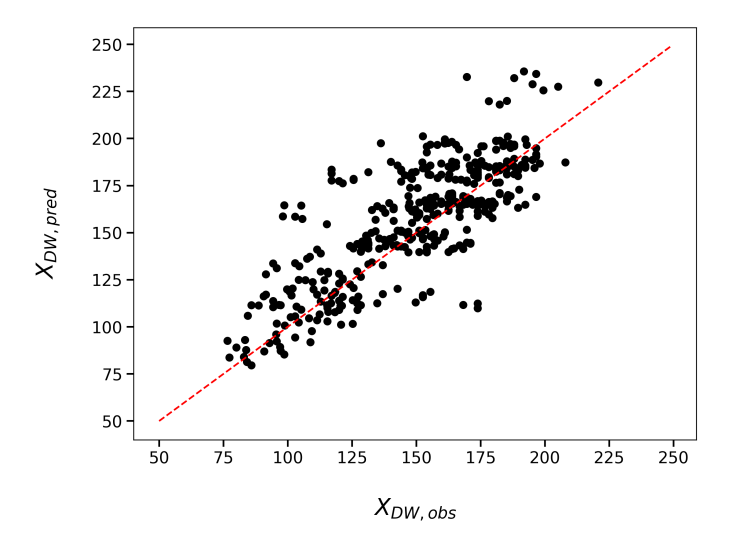


Figure 9: Commercial dataset: scatter plot comparing the predicted dry weight with the experimental measures.

We apply the aVH_{opt} model to the commercial dataset provided by Agricola Moderna, despite the substantial difference between this dataset and the research-oriented ones in Section 2.2, which suggests that suboptimal results may be expected.

Figure 9 compares the dry weight predictions with the corresponding experimental measurements. While the model successfully captures the overall trend of the observed data, it tends to predict the same value for several groups of data points, even when the corresponding experimental values show considerable variation. As a result, the performance of the model remains modest, with RMSE = 21.42 and

$$R^{2} = 1 - \frac{\sum_{i=1}^{N} (X_{DW,\text{obs}}^{i} - X_{DW,\text{pred}}^{i})^{2}}{\sum_{i=1}^{N} (X_{DW,\text{obs}}^{i} - \overline{X}_{DW,\text{obs}})^{2}} = 0.5,$$

indicating that a significant portion of the target variance is still unaccounted for. This limited performance may be due to the variability of certain environmental factors within the vertical farming facility that are not explicitly included in the model.

Motivated by the performance assessment in Figure 9, we further investigate which features most influence the mismatch between predicted and observed dry weight values.

To this end, consistently with Section 2.3.3, we employ a XGBoost regressor to estimate the prediction error and apply a Shapley value analysis to identify the environmental variables in the dataset that most contribute to the detected mismatch.

For training the XGBoost model, we consider as input features the duration of the growth cycle, detailed environmental data (temperature and relative humidity measured every 30 minutes), the substrate per plant, and the spatial position of the crop within the vertical farming unit. The output variable is the error between $X_{DW,\text{obs}}$ and $X_{DW,\text{aVH}_{\text{opt}}}$. Since temperature and relative humidity are time-dependent variables, we extract a set of statistical descriptors to track their general behavior over the whole growth period. These include: daily and nightly means and standard deviations, the daily range (i.e., the difference between maximum and minimum values over 24 hours), and the slope of the daily trend to measure how quickly temperature or humidity drop during the 20-hour LED light phase. In addition, we quantify the number of abrupt and moderate day-to-day variations in temperature and humidity. For temperature, variations between 1 [°C] and 2 [°C] are classified as moderate, while changes above 2 [°C] are considered significant. For relative humidity, moderate changes fall between 5% and 10%, and significant ones exceed 10%.

We optimize the hyperparameters of the regressor by dividing the dataset into three parts: 75% for training, 12.5% for validation, and the remaining 12.5% for testing. During this process, through stratification techniques, we ensure that the target variable distribution is balanced across all parts, so that the model learns and is evaluated fairly. The predictive performance of the trained model is characterized by $R^2 = 0.61$ and RMSE = 18.72. The results of the SHAP analysis are shown in Figure 10. It turns out that the three most influential factors affecting the prediction error of the aVH_{opt} model are all related to relative humidity, namely the daily variability, significant fluctuations during the growth cycle, and the overall range within 24 hours. This suggests that changes in relative humidity play a crucial role in crop development. Additionally, although to a lesser extent, the nightly mean and variability of temperature as well as substrate availability also impact the model. As a consequence, explicitly accounting for these three features in the aVH_{opt} model may lead to better prediction performance.

5 Conclusions

This paper proposes an approach to modeling plant growth by integrating the effects of light spectrum composition into a process-based model, making it suitable for vertical farming environments where light quality, among other environmental parameters, can be precisely regulated. Building on the crop growth model in [29], we introduce a data-driven adjustment that incorporates spectral information, i.e., the B:R and FR:R ratios, through a new parameter, γ , which captures how spectral composition influences growth. The optimization of parameter γ is performed jointly across multiple lettuce cultivars of *Lactuca sativa L.*, enabling a general characterization of the light spectrum role.

The aVH_{opt} model achieves a substantial improvement in predictive accuracy, consider-

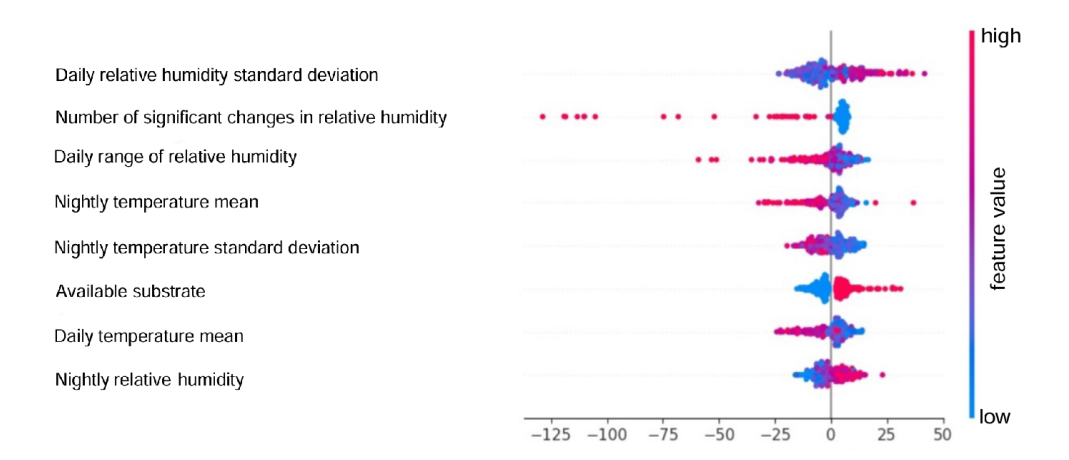


Figure 10: Commercial dataset: SHAP values associated with the key features driving the error between $X_{DW,\text{obs}}$ and $X_{DW,\text{aVH}_{\text{opt}}}$.

ably reducing RMSE on the validation set compared to the calibrated original formulation. These results underscore the importance of accounting for spectral quality when modeling plant growth and optimizing lighting strategies in vertical farming.

The application of the aVH_{opt} model to a commercial dataset highlights the impact of various biological and environmental features onto the plant development, beyond the light spectrum composition. For instance, different cultivars exhibit slightly different reactions to the same spectral ratios, and prediction accuracy decreases under more variable environmental conditions. These observations point to directions for future refinement. Further developments should include dedicated calibration for specific cultivars, as well as the incorporation of more biophysical knowledge (for instance, interactions between spectrum response and planting density via the Leaf Area Index). The analysis also suggests that additional variables, such as relative humidity and substrate availability, could significantly enhance model performance in commercial settings. Finally, coupling the model with real-time sensor data would enable continuous environmental optimization, supporting both crop performance and operational efficiency in vertical farming systems.

Declaration of competing interest

The authors declare that they have no known competing financial interests or personal relationships that could have appeared to influence the work reported in this paper.

Data availability

The data that has been used is confidential.

Acknowledgments

N.F. and S.P. are members of the Gruppo Nazionale Calcolo Scientifico Istituto Nazionale di Alta Matematica (GNCS-INdAM) and acknowledge the INdAM-GNCS 2025 project "Modelli Matematici Supportati dall'Integrazione di Dati per Agricoltura Sostenibile". S.M. and S.P. acknowledge the support by MUR, grant Dipartimento di Eccellenza 2023–2027. M.M. acknowledges the support of Agritech National Research Center and received funding from the European Union Next-GenerationEU (Piano Nazionale di Ripresa e Resilienza (PNRR) – Missione 4 Componente 2, Investimento 1.4 – D.D. 1032 17/06/2022, CN000000022).

References

- [1] X. Wang. Managing land carrying capacity: Key to achieving sustainable production systems for food security. *Land*, 11:484, 2022.
- [2] T. Gomiero. Soil degradation, land scarcity and food security: Reviewing a complex challenge. Sustainability, 8:281, 2016.
- [3] M.A.E. AbdelRahman. An overview of land degradation, desertification and sustainable land management using GIS and remote sensing applications. *Rendiconti Lincei. Scienze Fisiche e Naturali*, 34:767–808, 2023.
- [4] C. Ingrao, R. Strippoli, G. Lagioia, and D. Huisingh. Water scarcity in agriculture: An overview of causes, impacts and approaches for reducing the risks. *Heliyon*, 9:18507, 2023.
- [5] M. Tudi, H.D. Ruan, L. Wang, J. Lyu, R. Sadler, D. Connell, C. Chu, and D.T. Phung. Agriculture development, pesticide application and its impact on the environment. *International Journal of Environmental Research and Public Health*, 18:1112, 2021.
- [6] X. Zhu and L.F.M. Marcelis. Vertical farming for crop production. *Modern Agriculture*, 1:13–15, 2023.
- [7] T. Gerrewey, N. Boon, and D. Geelen. Vertical farming: The only way is up? *Agronomy*, 12:15, 2021.
- [8] X. Yuan, J. Hu, L.F.M. Marcelis, E. Heuvelink, J. Peng, X. Yang, and Q. Yang. Advanced technologies in plant factories: Exploring current and future economic and environmental benefits in urban horticulture. *Horticulture Research*, 12:5, 2025.
- [9] C. Banerjee and L. Adenaeuer. Up, up and away! The economics of vertical farming. Journal of Animal Science, 2:40–60, 2014.

- [10] M. Abedi, X. Tan, E.J. Stallknecht, E.S. Runkle, J.F. Klausner, M.S. Murillo, and A. Bénard. Incorporating the effect of the photon spectrum on biomass accumulation of lettuce using a dynamic growth model. Frontiers in Plant Science, 14:1525, 2023.
- [11] Q. Meng, N. Kelly, and E.S. Runkle. Substituting green or far-red radiation for blue radiation induces shade avoidance and promotes growth in lettuce and kale. *Environmental and Experimental Botany*, 162:383–391, 2019.
- [12] L. Carotti, A. Pistillo, I. Zauli, G. Pennisi, M. Martin, G. Gianquinto, and F. Orsini. Far-red radiation management for lettuce growth: Physiological and morphological features leading to energy optimization in vertical farming. *Scientia Horticulturae*, 334:113264, 2024.
- [13] K.J. McCree. The action spectrum, absorptance and quantum yield of photosynthesis in crop plants. *Agricultural Meteorology*, 9:191–216, 1972.
- [14] X.L. Chen, Q.C Yang, W.P. Song, L.C. Wang, W.Z. Guo, and X.Z. Xue. Growth and nutritional properties of lettuce affected by different alternating intervals of red and blue LED irradiation. *Scientia Horticulturae*, 223:44–52, 2017.
- [15] N. Claypool and J.H. Lieth. Physiological responses of pepper seedlings to various ratios of blue, green, and red light using LED lamps. Scientia Horticulturae, 268:109371, 2020.
- [16] Q. Meng, J. Boldt, and E.S. Runkle. Blue radiation interacts with green radiation to influence growth and predominantly controls quality attributes of lettuce. *Journal of the American Society for Horticultural Science*, 145:1–13, 2020.
- [17] X.L. Chen, Y.L. Li, L.C. Wang, and W.Z. Guo. Red and blue wavelengths affect the morphology, energy use efficiency and nutritional content of lettuce (Lactuca sativa L.). *Scientific Reports*, 11:8374, 2021.
- [18] J. Wang, W. Lu, Y. Tong, and Q. Yang. Leaf morphology, photosynthetic performance, chlorophyll fluorescence, stomatal development of lettuce (Lactuca sativa L.) exposed to different ratios of red light to blue light. Frontiers in Plant Science, 7:250, 2016.
- [19] G. Pennisi, F. Orsini, S. Blasioli, A. Cellini, A. Crepaldi, I. Braschi, F. Spinelli, S. Nicola, J.A. Fernandez, C. Stanghellini, G. Gianquinto, and L.F.M. Marcelis. Resource use efficiency of indoor lettuce (Lactuca sativa L.) cultivation as affected by red:blue ratio provided by LED lighting. *Scientific Reports*, 9:14127, 2019.
- [20] K.R. Cope and B. Bugbee. Spectral effects of three types of white light-emitting diodes on plant growth and development: Absolute versus relative amounts of blue light. Space Dynamics Laboratory Publications, 4:504–509, 2013.

- [21] Y. Saito, H. Shimizu, H. Nakashima, J. Miyasaka, and K. Ohdoi. The effect of light quality on growth of lettuce. *IFAC Proceedings Volumes*, 43:294–298, 2010.
- [22] K.H. Son and M.M. Oh. Leaf shape, growth, and antioxidant phenolic compounds of two lettuce cultivars grown under various combinations of blue and red light-emitting diodes. *HortScience*, 48:988–995, 2013.
- [23] S. Zhen and B. Bugbee. Substituting far-red for traditionally defined photosynthetic photons results in equal canopy quantum yield for CO₂ fixation and increased photon capture during long-term studies: Implications for re-defining PAR. Frontiers in Plant Science, 11:1, 2020.
- [24] S. Zhen and M.V. van Iersel. Far-red light is needed for efficient photochemistry and photosynthesis. *Journal of Plant Physiology*, 209:115–122, 2017.
- [25] Y. Chen, Z. Bian, L.F.M. Marcelis, E. Heuvelink, Q. Yang, and E. Kaiser. Green light is similarly effective in promoting plant biomass as red/blue light: a meta-analysis. *Journal of Experimental Botany*, 75:5655–5666, 2024.
- [26] K.H. Son and M.M. Oh. Increase in biomass and bioactive compounds in lettuce under various ratios of red to far-red LED light supplemented with blue LED light. Horticulture, Environment, and Biotechnology, 57:139–147, 2016.
- [27] W. Jin, J.L. Urbina, E. Heuvelink, and L.F.M. Marcelis. Adding far-red to red-blue light-emitting diode light promotes yield of lettuce at different planting densities. Frontiers in Plant Science, 11:609977, 2021.
- [28] J.A. Postma, V.L. Hecht, K. Hikosaka, E.A. Nord, T.L. Pons, and H. Poorter. Dividing the pie: A quantitative review on plant density responses. *Plant, Cell and Environment*, 44:1072–1094, 2021.
- [29] E.J. Van Henten. Validation of a dynamic lettuce growth model for greenhouse climate control. *Agricultural Systems*, 45:55–72, 1994.
- [30] 30MHz Support. How to apply PAR metrics in my widgets?, 2025. Accessed on 07-24, https://support.30mhz.com/hc/en-us/articles/360014617617-how-to-apply-par-metrics-in-my-widgets-.
- [31] X.Y. Wang, X.M. Xu, and J. Cui. The importance of blue light for leaf area expansion, development of photosynthetic apparatus, and chloroplast ultrastructure of Cucumis sativus grown under weak light. *Photosynthetica*, 53:213–222, 2015.
- [32] J.S. Lee and Y.H. Kim. Growth and anthocyanins of lettuce grown under red or blue light-emitting diodes with distinct peak wavelength. *Horticultural Science and Technology*, 32:330–339, 2014.

- [33] L. Yudina, E. Sukhova, M. Mudrilov, V. Nerush, A. Pecherina, A. Smirnov, A. Dorokhov, N. Chilingaryan, V. Vodeneev, and V. Sukhov. Ratio of intensities of blue and red light at cultivation influences photosynthetic light reactions, respiration, growth, and reflectance indices in lettuce. *Biology*, 11:60, 2022.
- [34] T. Chen and C. Guestrin. XGBoost: A scalable tree boosting system. In *Proceedings* of the 22nd ACM SIGKDD International Conference on Knowledge Discovery and Data Mining, 2016.
- [35] S.M. Lundberg and S.I. Lee. A unified approach to interpreting model predictions. In *Neural Information Processing Systems*, 2017.
- [36] L. Carotti, A. Pistillo, I. Zauli, G. Pennisi, M. Martin, G. Gianquinto, and F. Orsini. Far-red radiation management for lettuce growth: Physiological and morphological features leading to energy optimization in vertical farming. *Scientia Horticulturae*, 334:113264, 2024.
- [37] A. Trivellini, S. Toscano, D. Romano, and A. Ferrante. The role of blue and red light in the orchestration of secondary metabolites, nutrient transport and plant quality. *Plants*, 12:2026, 2023.
- [38] K. Ohashi-Kaneko, M. Takase, N. Kon, K. Fujiwara, and K. Kurata. Effect of light quality on growth and vegetable quality in leaf lettuce, spinach and komatsuna. *Environmental Control in Biology*, 45:189–198, 2007.
- [39] L. Li, Y. Tong, J. Lu, Y. Li, X. Liu, and R. Cheng. Morphology, photosynthetic traits, and nutritional quality of lettuce plants as affected by green light substituting proportion of blue and red light. *Frontiers in Plant Science*, 12:627311, 2021.
- [40] M. Naznin, M. Lefsrud, V. Gravel, and M. Azad. Blue light added with red LEDs enhance growth characteristics, pigments content, and antioxidant capacity in lettuce, spinach, kale, basil, and sweet pepper in a controlled environment. *Plants*, 8:93, 2019.

MOX Technical Reports, last issues

Dipartimento di Matematica Politecnico di Milano, Via Bonardi 9 - 20133 Milano (Italy)

- **45/2025** Caliò, G.; Ragazzi, F.; Popoli, A.; Cristofolini, A.; Valdettaro, L; De Falco, C.; Barbante, F. *Hierarchical Multiscale Modeling of Positive Corona Discharges*
- 44/2025 Brivio, S.; Fresca, S.; Manzoni, A.

 Handling geometrical variability in nonlinear reduced order modeling through Continuous
 Geometry-Aware DL-ROM
- 43/2025 Tomasetto, M.; Manzoni, A.; Braghin, F.

 Real-time optimal control of high-dimensional parametrized systems by deep-learning based reduced order models
- **41/2025** Torzoni, M.; Maisto, D.; Manzoni, A.; Donnarumma, F.; Pezzulo, G.; Corigliano, A. *Active digital twins via active inference*
- **42/2025** Franco, N. R.; Manzoni, A.; Zunino, P.; Hesthaven, J. S.

 Deep orthogonal decomposition: a continuously adaptive neural network approach to model order reduction of parametrized partial differential equations
- 40/2025 Tentori, C.A.; Gregorio, C.; ...; Ieva, F.; Della Porta, M.G.

 Clinical and Genomic-Based Decision Support System to Define the Optimal Timing of
 Allogeneic Hematopoietic Stem-Cell Transplantation in Patients With Myelodysplastic
 Syndromes
- 37/2025 Spreafico, M.; Ieva, F.; Fiocco, M.

 Causal effect of chemotherapy received dose intensity on survival outcome: a retrospective study in osteosarcoma
 - Gimenez Zapiola, A.; Boselli, A.; Menafoglio, A.; Vantini, S.

 Hyper-spectral Unmixing algorithms for remote compositional surface mapping: a review of the state of the art
- 35/2025 Perotto, S.; Ferro, N.; Speroni, G.; Temellini, E.

 Anisotropic recovery-based error estimators and mesh adaptation for real-life engineering innovation
- 34/2025 Bucelli, M.; Dede', L.

 Coupling models of resistive valves to muscle mechanics in cardiac fluid-structure interaction simulations